Chemical Physics Letters 501 (2011) 267–272

Contents lists available at ScienceDirect

Chemical Physics Letters

journal homepage: www.elsevier.com/locate/cplett

Optimal laser control of molecular photoassociation along with vibrational stabilization

Emanuel F. de Lima [a,*], Tak-San Ho [b], Herschel Rabitz [b]

[a] Departamento de Estatística, Matemática Aplicada e Computação, Instituto de Geociências e Ciências Exatas, Univ Estadual Paulista-UNESP, Rio Claro, São Paulo 13506-900, Brazil
[b] Department of Chemistry, Frick Laboratory, Princeton University, Princeton, NJ 08544, USA

ARTICLE INFO

Article history:
Received 4 November 2010
In final form 6 December 2010
Available online 9 December 2010

ABSTRACT

This work explores the optimization of laser pulses for the control of photoassociation and vibrational stabilization. Simulations are presented within a model system for the electronic ground-state collision of O + H. The goal is to drive the transition from a wavepacket representing the colliding atoms to the vibrational ground level of the diatomic molecule. The optimized fields resulting from two distinct trial pulses are analyzed and compared. Very high yields were obtained in the molecular vibrational ground-level.

1. Introduction

The control of photoassociation processes is a theme of considerable interest [1] with the basic case consisting of two colliding atoms interacting with an applied field to create a molecule. Photoassociation is a fundamental aspect of the laser control of chemical reactions [2] providing a means to create cold molecules starting from cooled atoms [3]. In most experimental situations, vibrationally highly excited molecules are produced, which may not be stable with respect to subsequent collisions. In order to obtain stable molecules, an important goal is the formation of molecules with low vibrational energy [4].

Photoassociation experiments have been performed with cw and pulsed lasers. Shaped laser pulses are especially attractive for controlling photoassociation dynamics because they provide broad bandwidth with frequency components that can be manipulated simultaneously [5]. A particular photoassociation experiment with femtosecond laser pulses worked with hot mercury atoms [6]. In the ultracold regime, electronically excited sodium molecules were formed using picosecond pulses [7]. Chirped nanosecond laser pulses have been applied to enhance the rate of inelastic collisions in an ultracold gas [8]. The utility of chirped femtosecond pulses was investigated in the formation of cold diatomic rubidium [9]. Recently, closed-loop experiments were performed to control the photoassociation of rubidium atoms with femtosecond pulses of low intensity [10]. Photoassociation with chirped pulses has also been considered theoretically [11,12]. In these latter works, the photoassociation involves the transition from a continuum state to an electronic excited state of a homonuclear molecule.

Here we consider photoassociation in the presence of infrared radiation to produce heteronuclear diatomic molecules directly in the electronic ground state. This process is driven by the laser interacting with the colliding atoms via the dipole moment associated with the collision. This phenomenon has been frequently described within a one-dimensional model system considering the Morse potential as the interatomic potential [13–18]. Early investigations [13,14] indicated the possibility of efficient vibrational state-selective association of O + H. The relation between the collision momentum and vibrational state-selective association of H + I has also been examined [15]. Those works were mainly concerned with the state-selective formation of highly excited vibrational levels and, as stated above, an important objective is occupation of much lower vibrational levels, especially the ground state. A recent investigation showed that multiphoton association can manipulate the population of intermediate vibrational levels by means of two pulses with commensurate carrier frequencies [16], but the population transfer to lower lying energy levels presented difficulties. A work on non-Markovian laser-driven association of OH in a environment showed that some population can be associated and eventually transferred to lower vibrational levels due to vibrational relaxation [19]. Local control theory was applied to study the photoassociation and vibrational stabilization of diatomic molecules, producing only small yields in the vibrational ground level even for a relatively long pulse of ten picoseconds [17,18]. The goal of this Letter is to show that quantum optimal control theory combined with fast monotonically convergent optimization algorithms can be invoked to find laser fields for effective

* Corresponding author. Fax: +55 1935269140.
E-mail addresses: eflima@rc.unesp.br (E.F. de Lima), tsho@princeton.edu (T.-S. Ho), hrabitz@princeton.edu (H. Rabitz).

0009-2614/$ - see front matter © 2010 Elsevier B.V. All rights reserved.
doi:10.1016/j.cplett.2010.12.018

control of photoassociation along with vibrational stabilization [20].

We consider the electronic ground-state collision of O + H coupled with the external laser field. Employing an accelerated monotonic algorithm formulated recently for optimizing the shape of control laser pulses [21], we show that very high yields can be obtained in the molecular ground vibrational energy level. We also analyze the optimal fields and corresponding population dynamics resulting from two different trial pulses.

2. General formulation

2.1. Collision model system

Consider the collision of two distinct atoms in the electronic ground state in the presence of a control field $\varepsilon(t), 0 \leqslant t \leqslant t_f$. The governing time-dependent Schrödinger equation in one-dimension can be written as

$$\imath\hbar\frac{\partial}{\partial t}\Psi(r,t) = [H_0 + H_1(t)]\Psi(r,t). \tag{1}$$

Here H_0 is the time-independent unperturbed molecular Hamiltonian,

$$H_0 = -\frac{\hbar^2}{2m_r}\frac{d^2}{dr^2} + V(r), \tag{2}$$

and H_1 is the interaction term

$$H_1(t) = -\mu(r)\varepsilon(t), \tag{3}$$

with r being the internuclear distance between the two colliding atoms and m_r, $V(r)$ and $\mu(r)$, respectively, being the underlying reduced mass, potential energy function, and dipole moment function. The initial state $\Psi(r,0)$ is taken as a Gaussian wavepacket

$$\Psi(r,0) = \left(\frac{2}{\pi a^2}\right)^{1/4}\exp\left[\imath k_0 r - (r-r_0)^2/a^2\right], \tag{4}$$

where r_0, $\hbar k_0 < 0$ and a are, respectively, the center of the wave packet, the relative momentum and the width of the wave packet. The dipole moment function $\mu(r)$ has the form

$$\mu(r) = qr\exp\left(-\frac{r}{r_d}\right), \tag{5}$$

where q is the effective charge and r_d denotes the range of the dipole interaction. The potential energy $V(r)$ is a Morse function truncated at long range L by an infinite barrier,

$$V(r) = \begin{cases} V_M(r), & \text{for } r \leqslant L \\ \infty, & \text{for } r > L \end{cases}. \tag{6}$$

The Morse function is

$$V_M(r) = D_e\left[e^{-2\alpha(r-r_e)} - 2e^{-\alpha(r-r_e)}\right], \tag{7}$$

where D_e is the well depth at the equilibrium position r_e, and α^{-1} is the potential range. The position of the barrier L is located sufficiently far outside the influence of the Morse oscillator, i.e., $L \gg (\alpha^{-1} + r_e)$ such that $V_M(L) \approx 0$. The eigenstates for the potential in Eq. (6) approach those of the standard Morse oscillator when the barrier is placed at long range. The introduction of the barrier allows for the calculations to employ square-integrable eigenstates as basis functions.

The set of eigenstates of the field-free Morse Hamiltonian H_0 is composed of bound states $\phi_v(r)$ with negative energies $-D_e < E_v < 0$ and scattering eigenstates $\phi_m(r)$ with positive energy $E_m > 0$. In order to notationally distinguish the scattering and bound states, the latter are labeled by the Greek letter $v = 0, 1, \ldots, N_b$, where N_b is the largest integer part of ζ, which satisfies the relation $2\zeta + 1 = \sqrt{8mrD_e}/(\hbar\alpha)$. The boundary condition imposed by the infinite wall implies discretization of the scattering states into a denumerably infinite set of levels. The quantization and proper normalization factor for the eigenfunctions at positive and negative energies has been derived [22]. For the bound states, the energy levels are given by $E_v = -[\hbar\alpha(N_b - v)]^2/(2m_r)$.

2.2. Time-dependent Schrödinger equation

The time-dependent equation Eq. (1) can be readily cast into matrix form by expanding the wave function $\Psi(r,t)$ in the energy bases $\phi_v(r)$ and $\phi_m(r)$ of H_0, i. e.,

$$\Psi(r,t) = \sum_{v=0}^{N_b} a_v(t)\phi_v(r) + \sum_{m=N_b+1}^{N} b_m(t)\phi_m(r), \quad N \gg N_b, \tag{8}$$

where the expansion coefficients $a_v(t)$ and $b_m(t)$ are, respectively, associated with the bound state $\phi_v(r)$ and the scattering state $\phi_m(r)$ with the normalization $\sum_{v=0}^{N_b}|a_v(t)|^2 + \sum_{m=N_b+1}^{N}|b_m(t)|^2 = 1\ \forall t \in [0,t_f]$. At $t = 0$, the expansion coefficients of the initial state function $\Psi(r,0)$ can be computed via the relations:

$$a_v(0) = \int_0^L \phi_v(r)\Psi(r,0)dr, \quad v = 0,1,\ldots,N_b, \tag{9}$$

and

$$b_m(0) = \int_0^L \phi_m(r)\Psi(r,0)dr, \quad m = N_b+1,\ldots,N, \tag{10}$$

where the initial wave function $\Psi(r,0)$ is given in Eq. (4). Consequently, substituting Eq. (8) into Eq. (1) yields the following first-order differential equation

$$\imath\hbar\frac{\partial}{\partial t}|\Psi(t)\rangle = (\mathbf{H}_0 - \boldsymbol{\mu}\varepsilon(t))|\Psi(t)\rangle, \tag{11}$$

where the time-dependent state $|\Psi(t)\rangle$ (a column vector) is composed of the expansion coefficients $a_v(t)$ and $b_m(t)$, the unperturbed Hamiltonian $\mathbf{H}_0$ is a diagonal matrix containing the bound energies E_v, $v = 0,1,\ldots,N_b$ and the discretized scattering energies E_m, $m = N_b+1,\ldots,N$. Analytical expressions for the dipole moment matrix elements $\{\mu_{vv'}, \mu_{vm}$ and $\mu_{mm'}\}$ are available for a variety of functional forms of $\mu(r)$ [22–24].

To solve Eq. (11), the corresponding propagator $U(t,0)$ may be written as

$$\begin{aligned} &U(t,0) = U(t,t-\Delta t)U(t-\Delta t,t-2\Delta t)\cdots U(2\Delta t,\Delta t)U(\Delta t,0), \\ &U(0,0) = \mathbf{I}, \end{aligned} \tag{12}$$

in terms of a sequence of propagators $U(\tau+\Delta t,\tau)$ over a short time step Δt. Each short-time propagator $U(\tau+\Delta t,\tau)$ can in turn be approximated by the second order split-operator expression

$$\begin{aligned} U(\tau+\Delta t,\tau) \approx &\exp\left(-\frac{\imath\mathbf{H}_0\Delta t}{2\hbar}\right)\times\exp\left(-\frac{\imath\boldsymbol{\mu}\varepsilon(\tau)\Delta t}{\hbar}\right) \\ &\times\exp\left(-\frac{\imath\mathbf{H}_0\Delta t}{2\hbar}\right), \end{aligned} \tag{13}$$

leading to the evolution of the state $|\Psi(\tau+\Delta t)\rangle = U(\tau+\Delta t,\tau)|\Psi(\tau)\rangle$. To evaluate the exponentials in Eq. (13), we only need to diagonalize the dipole matrix $\boldsymbol{\mu}$, since $\mathbf{H}_0$ is already diagonal.

2.3. Iterative numerical procedure for optimizing the control field

The control field $\varepsilon(t)$ can be efficiently optimized iteratively based on a family of recently formulated monotonically convergent

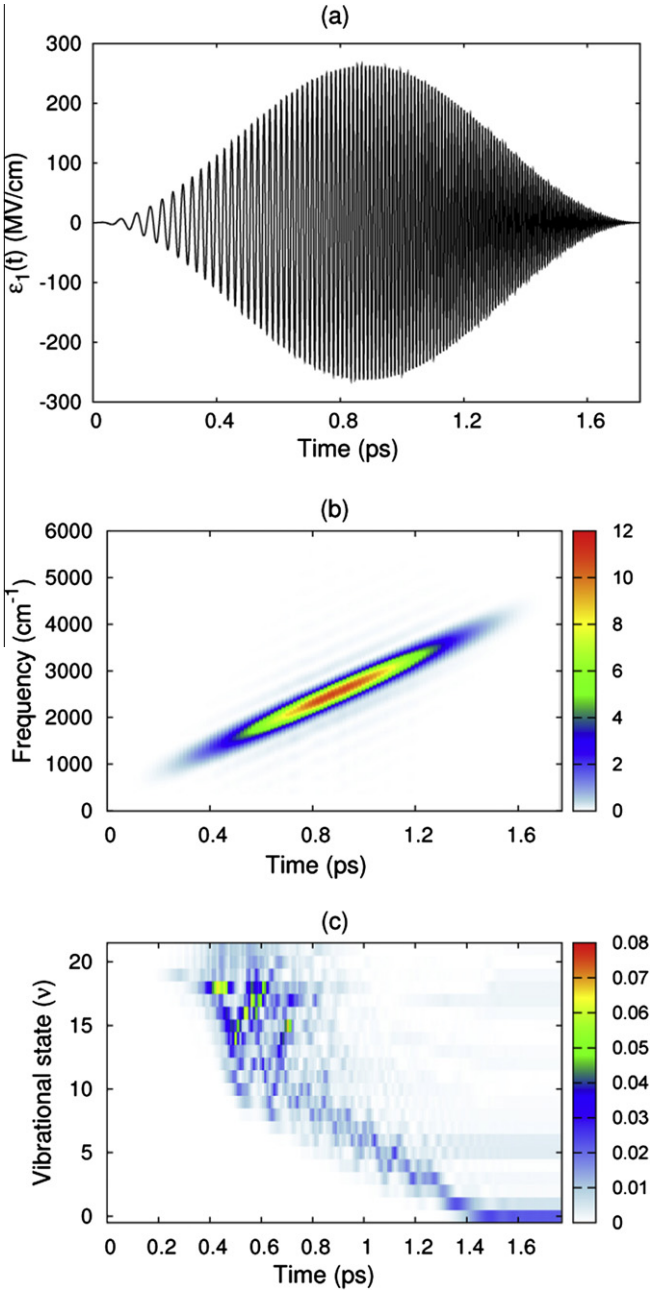

Figure 1. (a) The first trial field ε_1 in Eq. (20) and (b) the corresponding windowed Fourier transform (the colors indicate the windowed power spectrum in arbitrary units). (c) Population dynamics of the bound states (the colors indicate the population of each bound level).

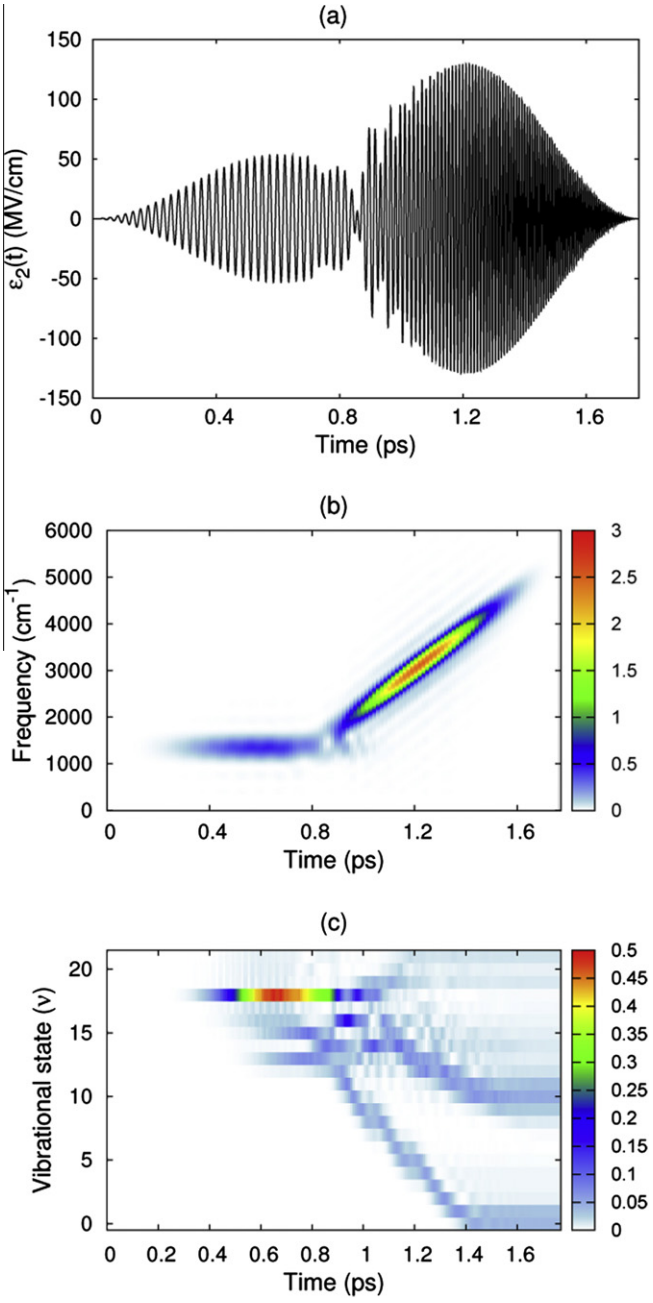

Figure 2. (a) Second trial field ε_2 in Eq. (22) and (b) the corresponding windowed Fourier transform (the colors indicate the windowed power spectrum in arbitrary units). (c) Population dynamics of the bound states (the colors indicate the population of each bound level).

iterative methods referred to as the two-point boundary-value quantum control paradigm (TBQCP) [21]. In this work, we will adopt the following particular TBQCP scheme (see [21] for details)

$$\varepsilon^{(1)}(t) = \varepsilon^{(0)}(t) + \eta S(t) f_\mu^{(1)}(t), \tag{14}$$

and

$$\varepsilon^{(n+1)}(t) = \varepsilon^{(n)}(t) + \eta S(t)\left\{2f_\mu^{(n+1)}(t) - f_\mu^{(n)}(t)\right\}, \quad n = 1, 2, \ldots, \tag{15}$$

for updating the control field $\varepsilon(t)$, starting with a trial control $\varepsilon^{(0)}(t)$, where $\eta > 0$ is a properly chosen step size for the iterations. The time interval $[0, t_f]$ is divided into M grid points $t_0 = 0, t_1, t_2, \ldots, t_{M-1}, t_M = t_f$ evenly spaced at Δt such that

$$f_\mu^{(n+1)}(t_i) = -\frac{2}{\hbar}\mathrm{Im}\langle \Psi^{(n+1)}(t_i)|\varphi_f^{(n)}(t_i)\rangle\langle\varphi_f^{(n)}(t_i)|\mu|\Psi^{(n+1)}(t_i)\rangle, \tag{16}$$

where

$$|\Psi^{(n+1)}(t_i)\rangle = U_{n+1}(t_i, t_i - \Delta t)|\{\Psi^{(n+1)}(t_i - \Delta t)\rangle,\ |\Psi^{(n+1)}(0)\rangle \equiv |\Psi(0)\rangle, \quad i = 1, 2, \ldots, M, \tag{17}$$

and

$$|\varphi_f^{(n)}(t_i)\rangle = U_n(t_i, t_i + \Delta t)|\varphi_f^{(n)}(t_i + \Delta t)\rangle,\ |\varphi_f(t_f)\rangle \equiv |f\rangle,\ \ i = 0, 1, \ldots, M-1. \tag{18}$$

The propagators $U_{n+1}(t_i, t_i - \Delta t)$ and $U_n(t_i, t_i + \Delta t)$ are, respectively, associated with the control field $\varepsilon^{(n+1)}(t)$ (being updated on the fly

at the current $(n+1)$th iteration) and the control field $\varepsilon^{(n)}(t)$ (at the previous nth iteration). $|\Psi(0)\rangle$ and $|f\rangle$ are, respectively, the initial and target quantum states. Before each new iteration, Eq. (18) is integrated backward numerically and the resultant $|\varphi_f^{(n)}(t_i)\rangle$, $i = M-1, M-2, \ldots, 2, 1, 0$, are stored for computing the function $f_\mu^{(n+1)}(t_i)$ in Eq. (16) while propagating the state $|\Psi(t_i)\rangle$ forward in time. The control field $\varepsilon(t)$ may also be filtered from iteration to iteration in order to eliminate unwanted frequency components, for instance, using a Butterworth bandpass filter [25]

$$h(\omega) = \left\{ \left[1 + \left(\frac{\omega_l}{\omega} \right)^{2m} \right] \left[1 + \left(\frac{\omega}{\omega_h} \right)^{2m} \right] \right\}^{-1/2}, \tag{19}$$

where ω_l and ω_h are respectively the low and high cutoff frequencies and m is the filter order.

3. Results and discussion

We consider the control field driven reaction $O + H \rightarrow OH$ where the initial state is described by the Gaussian wavepacket in Eq. (4) and the target state is the vibrational ground level $v = 0$. The objective is to maximize the expectation value of the projection operator $O_{t_f} = |\phi_0\rangle\langle\phi_0|$ at the final time $t = t_f$. The Morse potential parameters in Eq. (7) are [16,26] $D_e = 5.42$ eV (≈ 43763 cm^{-1}), $\alpha^{-1} = 0.445$ Å and the reduced mass is $m_r = 0.94$ amu. For those parameters the Morse oscillator has 22 bound states (i.e., the vibrational levels go from $v = 0$ to 21). The dipole function in Eq. (5) has the parameters $q = 1.634$—e— and $r_d = 0.6$ Å. The center of the initial wavepacket is $r_0 = 13.4$ Å and its width is 5.12 Å, so that at $t = 0$ the dipole moment is negligible in the region of the wavepacket. The position of the infinite barrier is set to $L = 47.63$ Å ≈ 90 au) and the initial relative kinetic energy $\hbar^2(k_0^2 + 1/a^2)/(2m_r) \approx 0.025$ eV (≈ 201.6 cm^{-1}) corresponds to a collision speed of ≈ 2.25 km/s, which is in the order of magnitude of atomic beam experiments [14]. Convergence for the calculations was found for $N = 362$ basis states and for the time-step $\Delta t = 0.295$ fs. In the following calculations, we consider trial fields consisting of up-chirped pulses based on (i) the structure of the bound vibrational levels, with an increasing energy gap between neighboring states for decreasing quantum number v and (ii) the goal of sweeping the packet down to the ground state in a multiphoton process. Two different trial fields are considered, with the first one being a single up-chirped pulse and the second one being a superposition of two pulses.

3.1. Outcome of the trial pulses

The first trial field is given by

$$\varepsilon_1(t) = S(t) \sin\left(\omega_c t + \frac{1}{2}\chi t^2 \right) \tag{20}$$

where $S(t)$ is

$$S(t) = \begin{cases} V \sin^2(\pi t/t_f), & \text{for } 0 \leqslant t \leqslant t_f \\ 0, & \text{otherwise.} \end{cases} \tag{21}$$

with $V = 263$ MVcm^{-1}, $t_f = 1.77$ ps, $\omega_c = 360$ cm^{-1}(≈ 10.8 ps^{-1}) and a linear chirp rate of $\chi = 464.5$ ps^{-2}. Panel (a) of Figure 1 shows the first trial field and its windowed Fourier transform is shown in

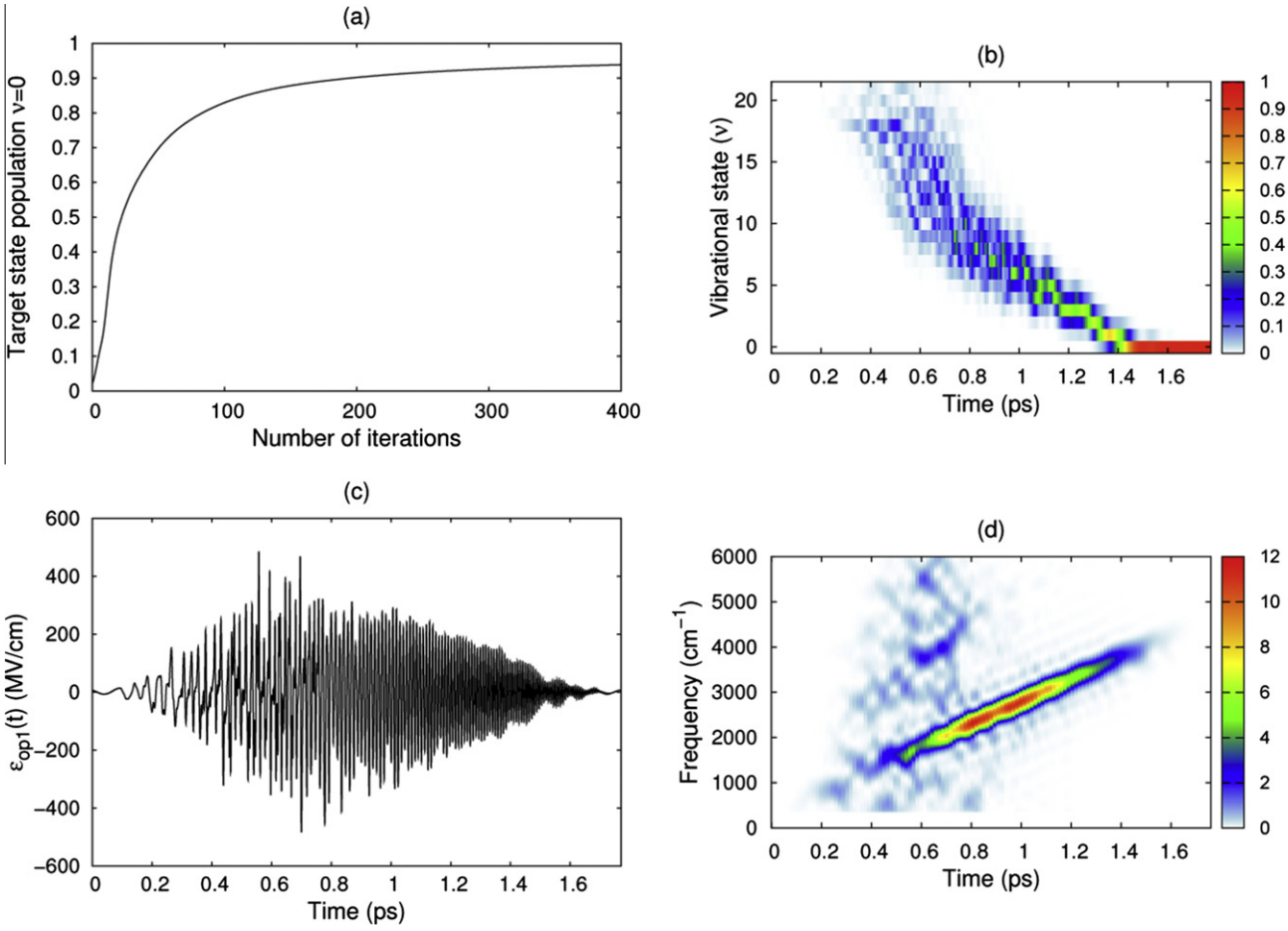

Figure 3. (a) Control calculations starting from the first trial field ε_1 (see Figure 1). (b) Population dynamics of the bound states (the colors indicate the population of each bound level). (c) Resulting control field and (d) the corresponding windowed Fourier transform (the colors indicate the windowed power spectrum in arbitrary units).

panel (b) where the pulse spectrum is very broad, ranging from $\sim 1000\ \mathrm{cm}^{-1}$ to $\sim 4000\ \mathrm{cm}^{-1}$. This frequency range includes the one-photon transitions from the average initial wavepacket energy to the bound states $v = 18$ to 15. Panel (c) shows the dynamics of the bound states upon application of this trial field. The bound state population is concentrated in the top levels $v > 10$ up to $t = 0.8$ and then the low lying states acquire some population. However, the total bound yield at the final time is only ≈ 0.05, and the target state population is just half of this value.

The second trial field consists of (i) a pulse with carrier frequency set to a specific free-to-bound transition frequency intended to enhance the photoassociation yield superimposed with (ii) a time-delayed up-chirped pulse aiming to perform vibrational stabilization,

$$\varepsilon_2(t) = S_1(t)\sin(\omega_1 t) + S_2(t)\sin\left[\omega_c(t-t_2) + \frac{1}{2}\chi(t-t_2)^2\right], \qquad (22)$$

where $S_i(t)$ $(i = 1, 2)$ are given by

$$S_i(t) = \begin{cases} V_i \sin\left[\pi \frac{(t-t_i)}{\Delta t_i}\right]^2, & \text{for } t_i \leqslant t \leqslant t_i + \Delta t_i \\ 0, & \text{otherwise.} \end{cases} \qquad (23)$$

We have set for the parameters for the unchirped pulse as $V_1 = 53\ \mathrm{MVcm}^{-1}$, $t_1 = 0$, $\Delta t_1 = 1.2$ ps and for the chirped pulse as $V_2 = 129.6\ \mathrm{MVcm}^{-1}$, $t_2 = 0.65$ ps and $\Delta t_2 = 1.12$ ps. The unchirped pulse is applied first and overlaps the chirped pulse. The carrier frequency of the first pulse $\omega_1 = 1354\ \mathrm{cm}^{-1}$ corresponds to the transition frequency from the average initial wavepacket energy to the bound vibrational state $v = 18$. The initial frequency of the chirped pulse is $\omega_c = 733\ \mathrm{cm}^{-1} (\approx 21.97\ \mathrm{ps}^{-1})$ and the linear chirp rate is $\chi = 800\ \mathrm{ps}^{-2}$. The total duration of the field is $t_f = 1.77$ ps.

Panel (a) of Figure 2 presents the second trial field. Its windowed Fourier transform in panel (b) shows that up to $t \approx 0.8$ ps the pulse spectrum is relevant only around the carrier frequency ω_1. As the chirped pulse enters, the frequency range becomes very broad, reaching above $4000\ \mathrm{cm}^{-1}$ at $t = t_f$. Panel (c) shows the dynamics of the bound states with this trial field. The $v = 18$ vibrational state acquires significant population up to the beginning of the chirped pulse, after which the population is spread over several intermediate states around $v = 10$ and several very low-lying states. The total bound population at the final time is ~ 0.3 and the population of the target $v = 0$ state is ~ 0.04.

3.2. Outcome of optimal control pulses

For the optimization calculations, we chose $\eta = 50$ in Eq. (14) and used a Butterworth filter of order $m = 25$ for which the low and high cut-off frequencies are respectively $\omega_l = 360\ \mathrm{cm}^{-1}$ and $\omega_h = 10700\ \mathrm{cm}^{-1}$. Figure 3a presents the results starting from the trial field ε_1 of Eq. (20). The target yield reaches 0.938 at the 400th iteration. Panel (b) shows the population dynamics of the bound states revealing a complex pattern of transfer from top states to bottom states with simultaneous occupation of several levels. Arrival of population in the ground state starts at $t \approx 1.4$ ps. The associated optimal control field $\varepsilon_{\mathrm{op1}}(t)$ and the corresponding windowed Fourier transform are depicted in panels (c)

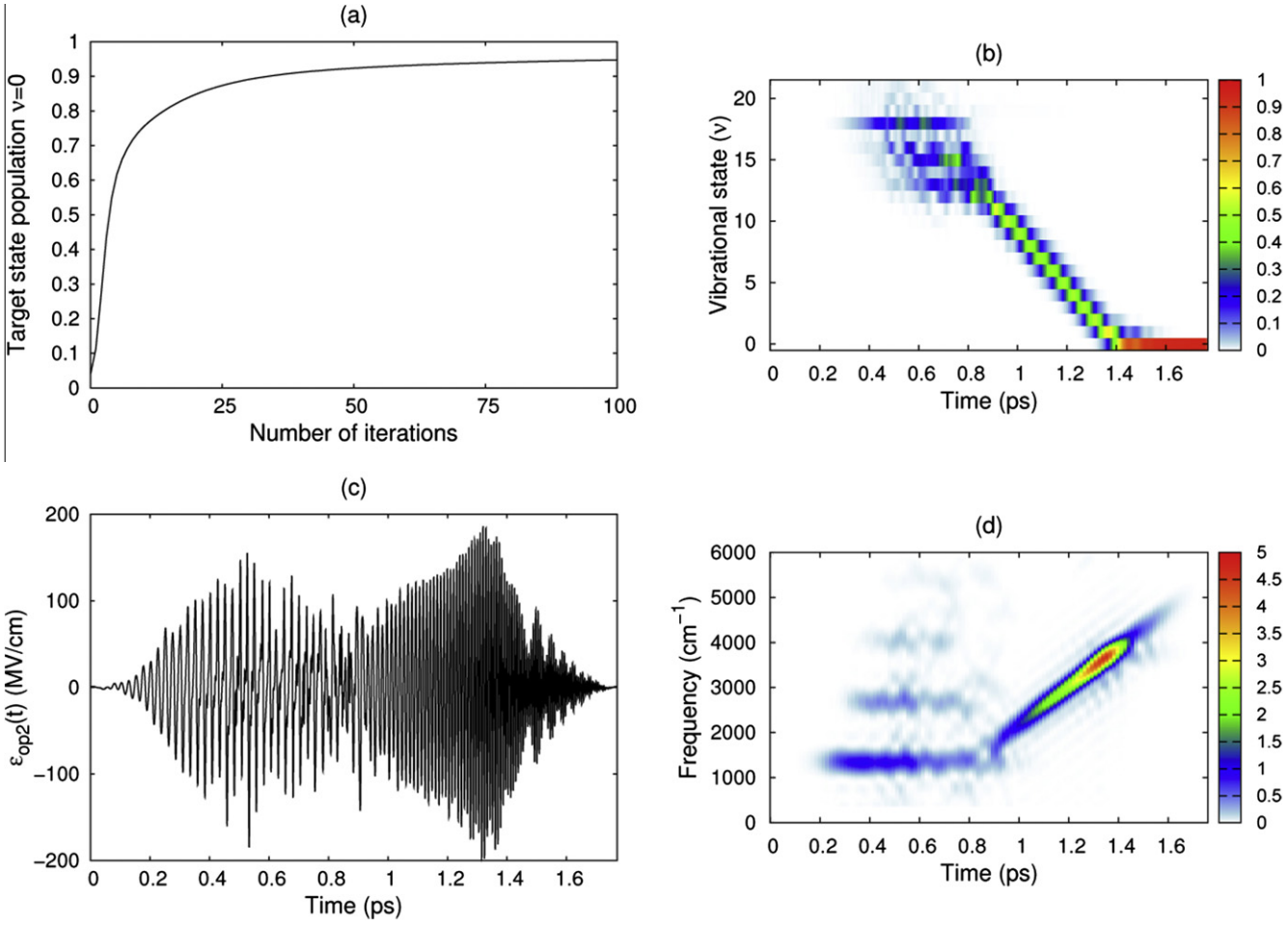

Figure 4. (a) Control calculations starting from the second trial field ε_2 (see Figure 2). (b) Population dynamics of the bound states (the colors indicate the population of each bound level). (c) Resulting control field and (d) the corresponding windowed Fourier transform (the colors indicate the windowed power spectrum in arbitrary units).

and (d), respectively. Upon comparing Figures 1b and 3d, it can be seen that a subtle pattern of frequencies from 360 cm^{-1} up to 6000 cm^{-1} appears in the optimized control field for $t < 0.8$ ps.

Figure 4a presents the results starting from the trial field ε_2 of Eq. (22). The target yield reaches 0.947 at the 100th iteration. Panel (b) show the population dynamics of the bound states. The $v = 18, 15, 16$ states participate in the initial period of the photoassociation process for $t < 0.8$ ps. Subsequently, there is ladder descent as corresponding to sequential population transfer from a vibrational state to the next immediately lower state, starting in the $v = 12$ state and reaching the ground state. Significant population in the ground state starts to appear at around $t = 1.4$ ps. The associated control field $\varepsilon_{op2}(t)$ and the corresponding windowed Fourier transform are depicted in panels (c) and (d), respectively. Upon comparing Figures 2b and 4d, it can be seen in that transition frequencies to the bound states $v = 16$ and 15 appear in the optimized control field for $t < 1$ ps, while they were not present in the original trial field.

Some general behavior is evident in the results. The chirped pulse chosen as the first trial field has not shown to be effective in performing the photoassociative transition from a scattering state (here in terms of a moving Gaussian wavepacket) to the lowest bound vibrational level. It is attractive to initially perform a transition to a high-lying vibrational level, as indicated in previous works [13,16]. However, it is still difficult to produce a significant transition to the ground vibrational state even by appending an additional intuitive up-chirped pulse, as shown in Figure 2. Subsequent optimization of the trial pulses ε_1 and ε_2 proved to be very effective. These results indicate that effective laser pulses may be found for both photoassociation and vibrational stabilization upon proper shaping.

Some additional insights can be drawn from the effort required to search for the optimal field in the two trials. The number of iterations needed to reach the same yield with ε_1 was four times greater than for ε_2, as seen in comparing Figures 3a and 4a. Furthermore, the peak intensity of the resulting optimized field $\varepsilon_{op1}(t)$ was considerably greater then for $\varepsilon_{op2}(t)$. These differences are reflected in the distinct mechanisms of the stabilization process for the two cases, evident in comparing Figures 3b and 4b. The existence of such multiple solutions is consistent with quantum control landscape analysis [27,28]. Comparisons between the windowed Fourier transform of the optimized fields with that of the respective initial trial fields also reveals that the corresponding optimal solutions tend to depart from the initial trial fields in subtle ways. All of these points highlight the relevant role played by the initial trial field. Although in principle any trial field can be the seed leading to an optimal solution, the efficiency of the search, the form of the final field and the control mechanism can notably depend on the trial field.

4. Conclusions

We have optimized laser pulses for the control of photoassociation along with vibrational stabilization in a model system for the electronic ground-state collision of O + H. Optimal controls were found by starting from a wavepacket at a large internuclear distance with the objective being to maximize the population of the vibrational ground state $v = 0$ at a particular time. We found that very high yields (at least 0.947 of the norm of the initial state) can be obtained with optimized pulses acting on a time scale of less than 2 ps. This result may be compared with significantly lower yields produced by pulses obtained from local control theory in a similar system [17,18]. Finally, we hope that this work stimulates further investigations into photoassociation and vibrational stabilization in more complex systems, which may include additional partial waves, molecular rotation, electronic degrees of freedom and thermal effects.

Acknowledgments

This work was partially supported by the Conselho Nacional de Desenvolvimento Científico e Tecnológico (CNPq), Brazil. We express our acknowledgment to M.A.M. de Aguiar for providing access to computer facilities. This work was partially developed in the group of V.S. Bagnato of the Instituto de Física de São Carlos – USP, Brazil. T.-S. Ho and H. Rabitz acknowledge support by the U.S. Department of Energy.

References

[1] K.M. Jones, E. Tiesinga, P.D. Lett, P.S. Julienne, Rev. Mod. Phys. 78 (2006) 483.
[2] R.N. Zare, Science 279 (1998) 1875.
[3] J.M. Sage, S. Sainis, T. Bergeman, D. DeMille, Phys. Rev. Lett. 94 (2005) 203001.
[4] C.P. Koch, J.P. Palao, R. Kosloff, F. Masnou-Seeuws, Phys. Rev. A 70 (2004) 013402.
[5] H. Rabitz, R. Vivie-Riedle, M. Motzkus, K. Kompa, Science 288 (2000) 824.
[6] U. Marvet, M. Dantus, Chem. Phys. Lett. 245 (1995) 393.
[7] F. Fatemi, K.M. Jones, H. Wang, I. Walmsley, P.D. Lett, Phys. Rev. A 64 (2001) 033421.
[8] M.J. Wright, S.D. Gensemer, J. Vala, R. Kosloff, P.L. Gould, Phys. Rev. Lett. 95 (2005) 063001.
[9] B.L. Brown, A.J. Dicks, I.A. Walmsley, Phys. Rev. Lett. 96 (2006) 173002.
[10] W. Salzmann, U. Poschinger, R. Wester, M. Weidemüller, A. Merli, S.M. Weber, F. Sauer, M. Plewicki, F. Weise, A.M. Esparza, et al., Phys. Rev. A 73 (2006) 023414.
[11] J. Vala, O. Dulieu, F. Masnou-Seeuws, P. Pillet, R. Kosloff, Phys. Rev. A 63 (2000) 013412.
[12] E. Luc-Koening, R. Kosloff, F. Masnou-Seeuws, M. Vatasescu, Phys. Rev. A 70 (2004) 033414.
[13] M.V. Korolkov, J. Manz, G.K. Paramonov, B. Schmidt, Chem. Phys. Lett. 260 (1996) 604.
[14] M.V. Korolkov, B. Schmidt, Chem. Phys. Lett. 272 (1997) 96.
[15] Y.-Y. Niu, S.-M. Wang, S.-L. Cong, Chem. Phys. Lett. 428 (2006) 7.
[16] E.F. de Lima, J.E.M. Hornos, Chem. Phys. Lett. 433 (2006) 48.
[17] P. Marquetand, V. Engel, J. Chem. Phys. 127 (2007) 084115.
[18] P. Marquetand, V. Engel, J. Phys. B 41 (2008) 074026.
[19] G.K. Paramonov, P. Saalfrank, Phys. Rev. A 79 (2009) 013415.
[20] S. Shi, H. Rabitz, J. Chem. Phys. 92 (1990) 364.
[21] T.-S. Ho, H. Rabitz, Phys. Rev. E 82 (2010) 026703.
[22] E.F. de Lima, T.-S. Ho, H. Rabitz, J. Phys. A 41 (2008) 335303.
[23] E.F. de Lima, J.E.M. Hornos, J. Chem. Phys. 125 (2006) 164110.
[24] E.F. de Lima, J.E.M. Hornos, J. Phys. B 38 (2005) 815.
[25] S. Butterworth, Exp. Wireless Wireless Eng. 7 (1930) 536.
[26] E.F. de Lima, T.-S. Ho, H. Rabitz, Phys. Rev. A 78 (2008) 063417.
[27] H.A. Rabitz, M.M. Hsieh, C.M. Rosenthal, Science 303 (2004) 1998.
[28] H.A. RabitzM.M. Hsieh, R. Kosut, M. Demiralp, Phys. Rev. A 74 (2006) 012721.